



**HAL**  
open science

## Can fossil bones and teeth be dated using fission track analysis?

Marc Jolivet, Anne-Élisabeth Lebatard, Jean-Louis Reyss, Didier Louis Bourlès, Hassane Taïso Mackaye, Fabrice Lihoreau, Patrick Vignaud, Michel Brunet

### ► To cite this version:

Marc Jolivet, Anne-Élisabeth Lebatard, Jean-Louis Reyss, Didier Louis Bourlès, Hassane Taïso Mackaye, et al.. Can fossil bones and teeth be dated using fission track analysis?. *Chemical Geology*, 2008, 247 (1-2), pp.81-99. 10.1016/j.chemgeo.2007.10.009 . hal-00411880

**HAL Id: hal-00411880**

**<https://hal.science/hal-00411880>**

Submitted on 4 May 2022

**HAL** is a multi-disciplinary open access archive for the deposit and dissemination of scientific research documents, whether they are published or not. The documents may come from teaching and research institutions in France or abroad, or from public or private research centers.

L'archive ouverte pluridisciplinaire **HAL**, est destinée au dépôt et à la diffusion de documents scientifiques de niveau recherche, publiés ou non, émanant des établissements d'enseignement et de recherche français ou étrangers, des laboratoires publics ou privés.



Distributed under a Creative Commons Attribution - NonCommercial - NoDerivatives 4.0 International License

# Can fossil bones and teeth be dated using fission track analysis?

M. Jolivet <sup>a,\*</sup>, A.-E. Lebatard <sup>b</sup>, J.-L. Reyss <sup>c</sup>, D. Bourlès <sup>d</sup>, H.T. Mackaye <sup>e</sup>,  
F. Lihoreau <sup>e</sup>, P. Vignaud <sup>b</sup>, M. Brunet <sup>b</sup>

<sup>a</sup> *Laboratoire Géosciences Montpellier, UMR CNRS 5573 Université Montpellier II, France*

<sup>b</sup> *Laboratoire de Géobiologie, Biochronologie et Paléontologie Humaine, UMR CNRS 6046, Université de Poitiers, France*

<sup>c</sup> *Laboratoire des Sciences du Climat et de l'Environnement, UMR CNRS-CEA 1572, Gif sur Yvette, France*

<sup>d</sup> *C.E.R.E.G.E., UMR CNRS—Université Paul Sézanne, Aix en Provence, France*

<sup>e</sup> *Département de Paléontologie, Université N'Djamena, N'Djamena, Chad*

he high proportion of crystallized apatite forming the bones and teeth should theoretically allow the use of fission track analysis to date vertebrate fossils when burying of the fossiliferous series did not subject them to temperatures exceeding 60 °C. However several major obstacles arise such as the complexity of fossils' internal structures, diagenetic modifications and substitutions of the hydroxyapatite by other minerals, and massive U uptake or loss during diagenesis. In this work, those various problems are addressed combining optical microscope observation of the fossils, a systematic fission track analysis of the best samples,  $\alpha$  and  $\gamma$  spectrometry and Secondary Ion Mass Spectrometry. Even if the problems caused by internal structures and mineral substitutions can be solved, U movements in and out of the fossils are generally too complex to allow fission track analysis dating of the fossils.

*Keywords:* Uranium series; Fission track analysis; Fossils; Diagenesis

## 1. Introduction

Fission track analysis (FTA) is a low temperature thermochronology method largely used to study geological processes such as relief building, erosion, sedimentation or tectonic movements (e.g. Gleadow and Brown, 2000; Jolivet et al., 2001, 2007; Sobel et al., 2006). Although minerals like zircon and titanite are sometimes analysed using FTA (e.g. Tagami et al.,

1996; Tagami and Shimada, 1996; Dahl, 1997; Coyle and Wagner, 1998; Jolivet et al., 2001), the method is mostly applied on apatite.

Fission tracks are intra-crystalline defects produced by radiation damages following the spontaneous nuclear fission of  $^{238}\text{U}$  atoms. Through time those damages are progressively annealed with a rate depending upon the chemical composition of the mineral and the temperature (e.g. Green et al., 1986; O'Sullivan and Parrish, 1995; Barbarand et al., 2003). In apatite, for temperatures lower than ca. 110 °C, annealing rates become sufficiently low so that fission tracks remain in the

\* Corresponding author. Tel.: +33 4 67 14 37 00; fax: +33 4 67 14 36 42.  
E-mail address: jolivet@gm.univ-montp2.fr (M. Jolivet).

crystal during geologically significant periods. Below 60 °C, annealing rates are so slow that they have no effect on the fission tracks at geological time scales (Green et al., 1986).

Bones are formed by 70% of phosphatic minerals associated with organic material. The mineral fraction is mainly hydroxyapatite that forms sub-micrometric crystals or fibres (Michel et al., 1997; Pfretzschner, 2004). Teeth dentine presents an open porosity and chemical composition similar to those of the bones but generally the mineral fraction is slightly higher. Teeth enamel is also composed of hydroxyapatite but with a higher degree of crystallinity and only about 2% of organic material (Michel et al., 1997 and references therein). This high proportion of crystallized apatite should allow the use of FTA to determine the age of fossil bones and teeth when burying of the fossiliferous

series did not subject them to temperatures exceeding 60 °C.

Sachs et al. (1980) applied FTA to conodont fossils. They concluded that the method could be relevant but because of the low U concentration in their fossils (less than 1 ppm), the results were not accurate. Modern bones and teeth usually contain a few ppb of U (Iyengar et al., 1978) which is too low to apply the FTA method even on very old (several 100 Ma) samples. But buried bones and teeth have the ability to take up large amounts of U (up to several hundreds of ppm) from their surrounding environment (e.g. Millard and Hedges, 1996; Pike et al., 2002; Van Calsteren and Thomas, 2006). This process of U uptake through time can be further complicated by periods of U loss caused by variations in the environmental parameters (e.g. Rae et al., 1989; Hoffmann and Mangini, 2003).

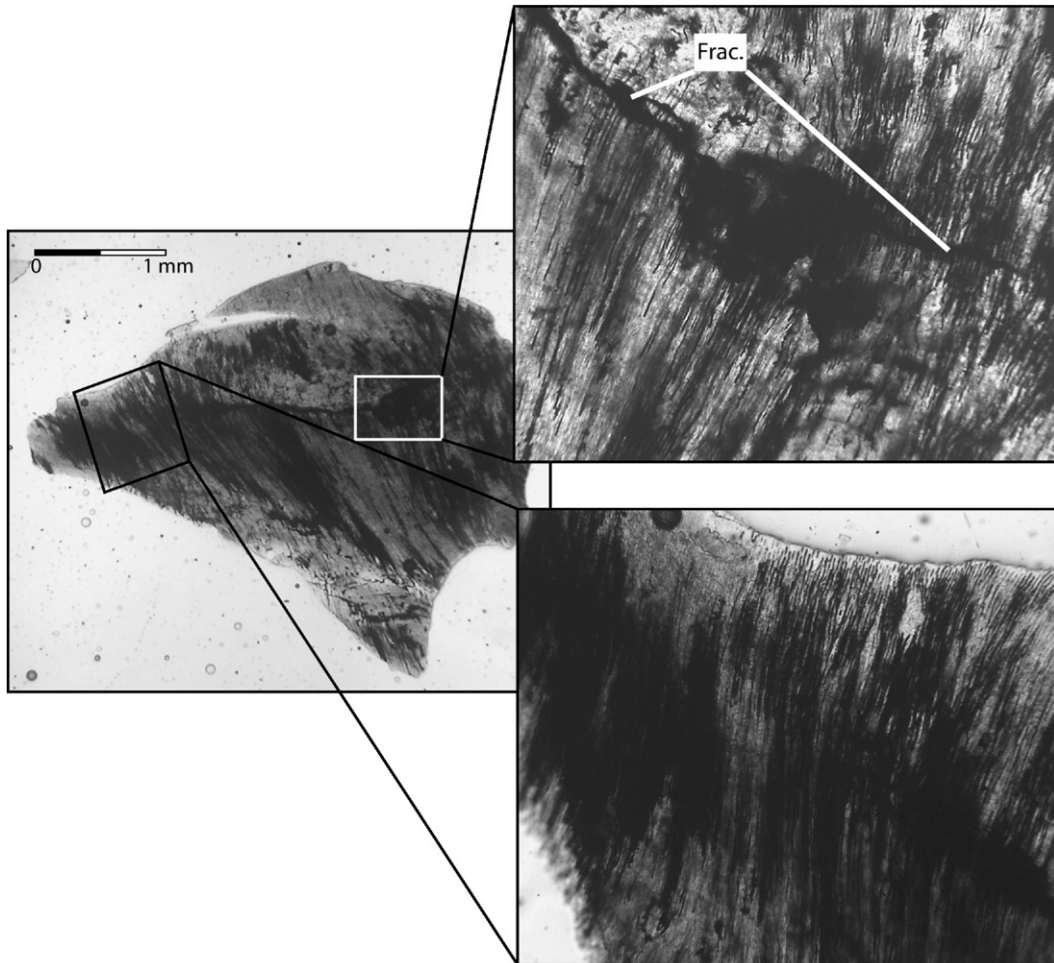


Fig. 1. Fragment of Proboscidean tooth from Chad (sample KB3-10 from Mio-Pliocene of Kossom Bougoudi), showing a high proportion of diagenetic oxides. Diagenetic minerals are present both in mechanical fractures (Frac.) and within internal structures such as the Tomes canals that allow the fluids present in the external environment to circulate inside the fossil.

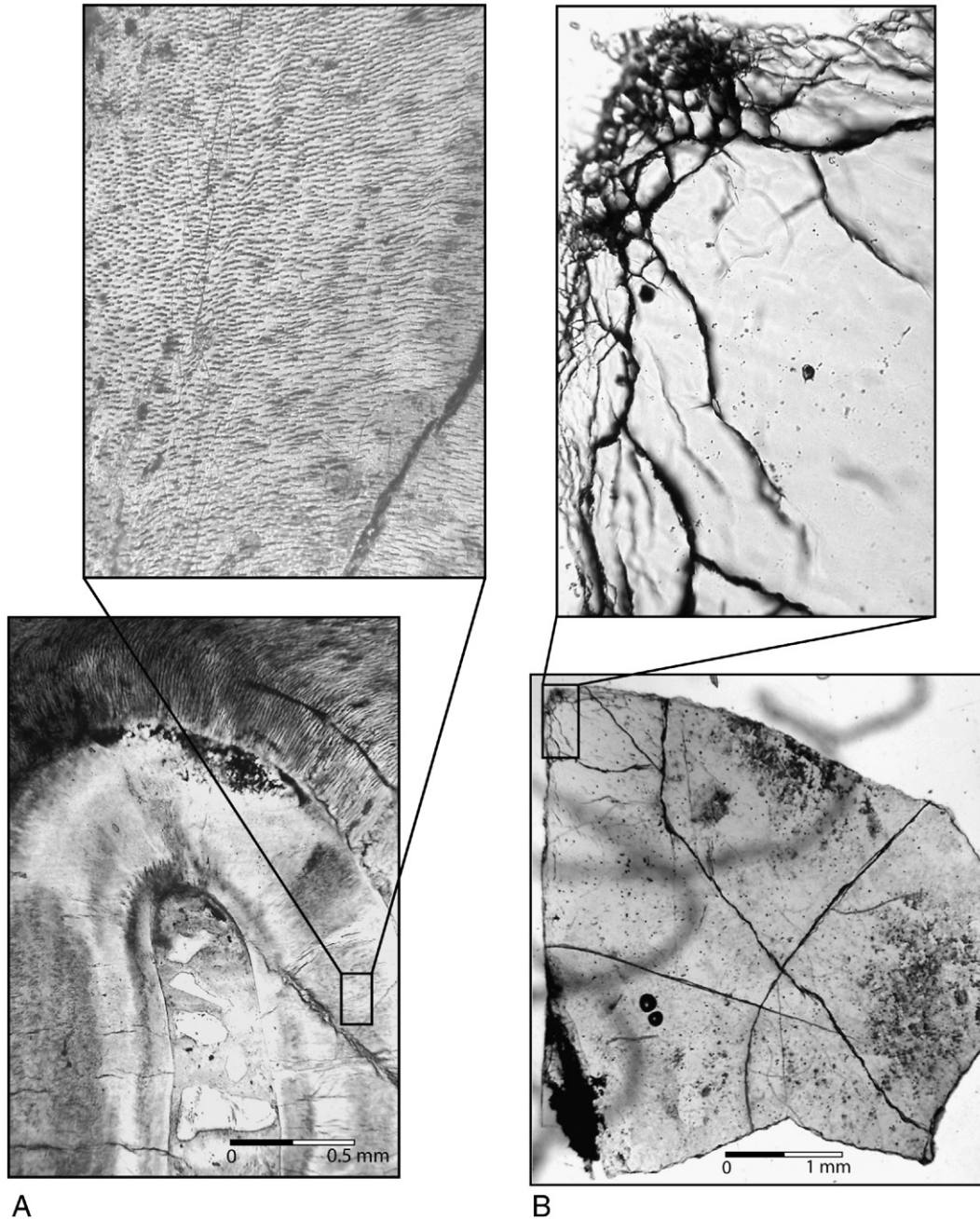


Fig. 2. Examples of prismatic (A) and aprismatic (B) enamel. Prismatic enamel (Bovid tooth from the Late Miocene Toros-Menalla site (TM 266) in Chad) is especially characterized by the occurrence of the Tomes canals (small black lines and dots on the expanded image) which have approximately the same size as the fission tracks and thus prevent any rigorous fission track analysis. Aprismatic enamel (Actinopterygian scale, Cenomanian, Morocco) appears to be a much better material for fission track analysis as it does not display any apparent internal structures.

Millard and Hedges (1996) proposed a Diffusion-Adsorption model to describe the uptake of U in bones. Under oxic conditions, complexes of the uranyl ion ( $\text{UO}_2^{2+}$ ) diffuse into the bone porous structure and are adsorbed onto the internal surface area of the mineral

fraction. This leads to U concentration decreasing from the edge of the bone towards the inside creating a  $\bar{E}$  shaped "concentration profile". When the bone reaches equilibrium, the concentration is similar all over the structure. However, this model is only valid for a short

period of time after burial and certainly not over millions of years (Millard and Hedges, 1996). It is widely used for TIMS, Laser ablation ICP-MS and ESR dating of archeological bones (e.g. Pike and Hedges, 2001; Pike et al., 2002; Eggins et al., 2003; Hoffmann and Mangini, 2003; Van Calsteren and Thomas, 2006 and references therein).

The application of FTA on fossils relies on the fact that all the U present within the fossils is incorporated during early diagenetic processes, i.e. within a period of time negligible compared to the age of the sample. If this is usually the case for young samples (Millard and Hedges, 1996; Michel et al., 1999) or for samples with a very simple diagenetic history, fossils may also incorporate or lose U during late diagenetic events. Only in the first case the FTA age will be close to the stratigraphic age of the fossil.

In this paper we address the feasibility of FTA on biogenic fossil apatite paying a particular attention to three major obstacles:

- Occurrence of internal structures within the samples: minerals analysed by FTA must be etched to reveal the fission tracks (e.g. Hurford and Green, 1983). In the case of fossils, etching also reveals the micrograin boundaries and other internal structures, potentially blackening the sample and hiding the fission tracks (Sachs et al., 1980).
- During diagenesis, and especially during early diagenesis, new mineral phases such as quartz, calcite and oxide will develop inside the fossil (e.g. Sharma et al., 1981), either dramatically decreasing the amount of apatite in the sample or, for the oxides, hiding the possible occurrence of fission tracks (Fig. 1).
- Finally, as said before U is usually massively incorporated (and sometimes lost) during diagenesis. It is thus important to understand the long term evolution (several Ma) of the U concentration in the fossil as well as its relations with the diagenetic minerals.

## 2. Methodology

In order to select the best type of fossils to be used for FTA, a large range of samples such as fish, reptiles and mammal bones and teeth were tested. Those samples represent a large range of deposition ages and fossilization environments. They were provided by the French National Museum of Natural History (MNHN) and the Mission Paléontologique Franco-Tchadienne (MPFT).

Observation of spontaneous fission tracks within apatite requires revealing the latent tracks by etching using a 6.5% HNO<sub>3</sub> solution (Hurford and Green, 1983). However other structures inside the crystal (cracks, inclusions, etc.) are also etched. Artificially enhanced internal structures of bones and teeth (e.g. Tomes canals, Haversian canals and microcrystallite joints) may thus be a major problem for fission track observations (Sachs et al., 1980). To assess this problem, we compared bones, dentine, prismatic enamel (fibrous structure) and aprismatic enamel (no apparent structure) (Fig. 2).

The effect of diagenesis on the occurrence of fission tracks was tested using the largely diagenetically modified Mio-Pliocene samples from the Chad basin (Brunet et al., 2005 and references therein). These samples set includes teeth, bones osteodermis and scales of fish (Siluriformes), reptiles (ex: Crocodylidae) and mammals (Proboscidea, Anthracotheriidae, etc.). Most samples are black or dark brown due to a large concentration of diagenetic oxides and they have been largely silicified during diagenesis. Stratigraphic ages vary from ca.7 Ma in Toros-Ménalla (TM) to 5.5–4.5 Ma in Kossom Bougoudi (KB), 5–4 Ma in Kollé (KL) and 3.5–3 Ma in Koro Toro (KT) (Fig. 3). A preliminary  $\gamma$  spectrometry study showed mean U concentration of more than 100 ppm for the Chadian samples, much higher than the usual concentration found in modern bones and teeth (e.g. Iyengar et al., 1978). This, together with the large amount of oxides and silica within the samples, implies strong diagenetic processes (Fig. 1).

U concentrations within various discrete areas of the fossils were calculated from induced fission track counting. To allow an independent control on the results, they were compared to U and Th mean concentration obtained by  $\alpha$  and  $\gamma$  spectrometry and to precise maps of U and Th distribution obtained using Secondary Ion Mass Spectrometry (SIMS). Furthermore, Ca, P, K, Al, Si and Mn distribution maps obtained by SIMS were used to evaluate the intensity of the diagenetic processes.

## 3. Sample preparation

### 3.1. Fission track analysis

Samples were cut along transverse and longitudinal sections to allow observation of the various internal structures. For some of the fossils, small fragments with various orientations were also used. Polished thin sections, about 50  $\mu$ m thick were made and analysed

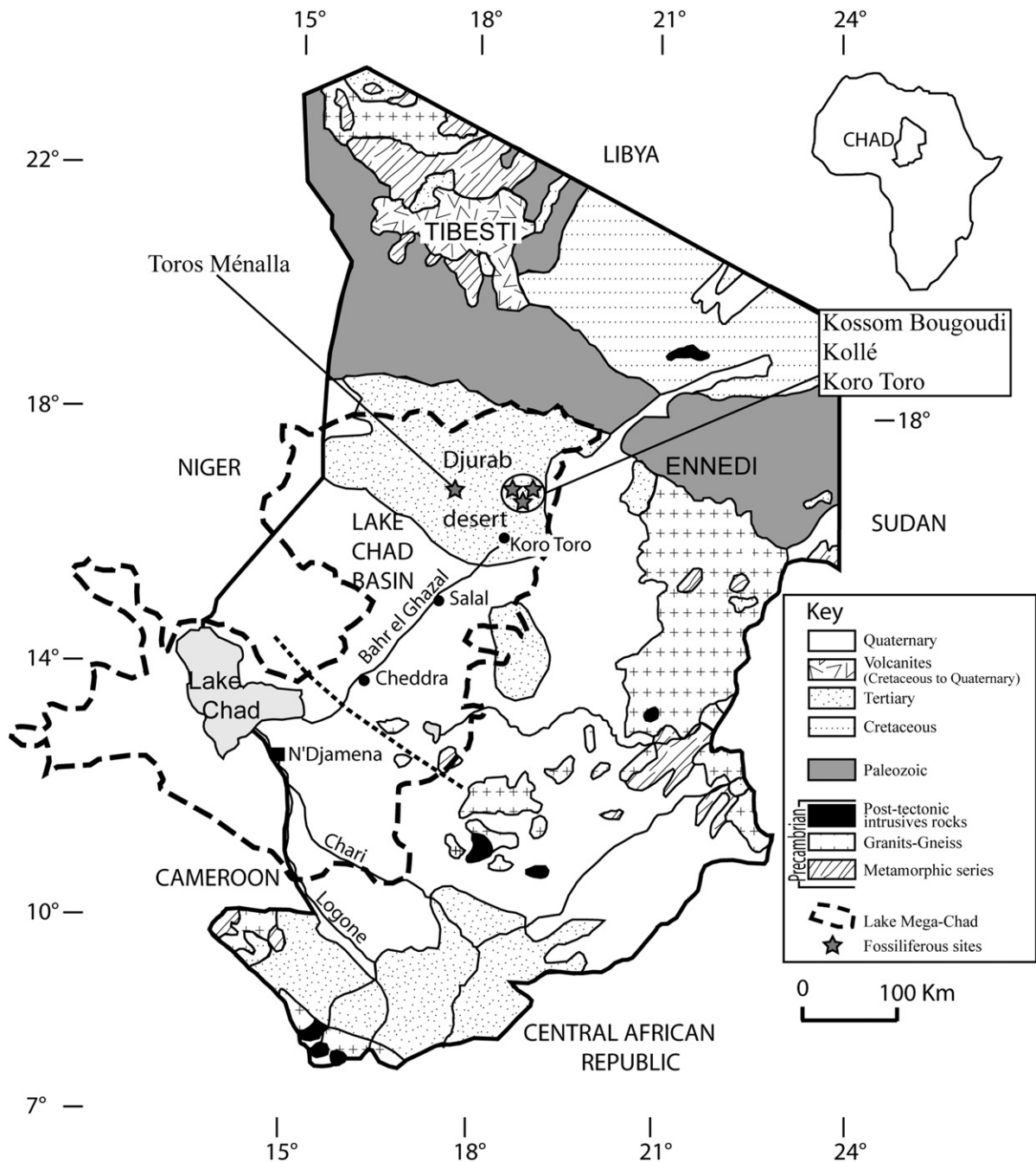


Fig. 3. Schematic structural and geological map of Chad with localization of the Mio-Pliocene fossiliferous area (map modified from Kusnir and Moutaye, 1997).

in transmitted, reflected and polarized light on a Zeiss Axioplan II optical microscope.

Preparation of the samples for FTA mostly follows the methodology described in Hurford and Green (1983) and Hurford (1990). Samples were etched in 6.5%  $\text{HNO}_3$  for 45 s at 20 °C to reveal the spontaneous fission

tracks. Etching also revealed the internal structures of the fossils which most of the time blacken the surface of the sample impeding microscopic observation (Fig. 4). To partially solve that problem without erasing the potential fission tracks, 1  $\mu\text{m}$  of material was removed from the surface using 0.03  $\mu\text{m}$  grain size aluminium

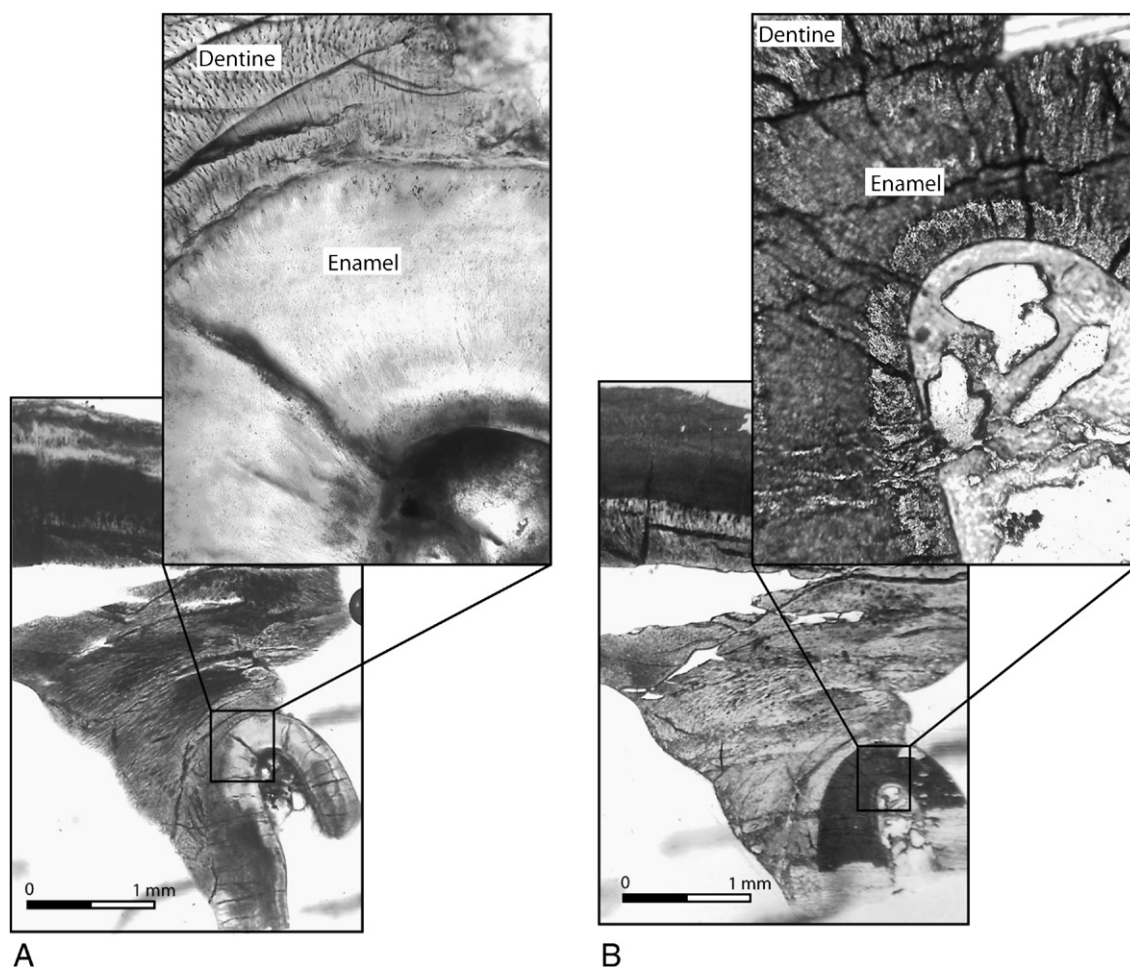


Fig. 4. Effect of etching upon internal structures in mammalian tooth samples. Fig. 3A shows a thin section of Bovid tooth (TM266, Late Miocene, Chad) in longitudinal cut prior to etching. Most of the visible internal structures are situated inside the dentine and the enamel appears clear as even the Tomes canals are not clearly visible. After etching using 6.5%  $\text{HNO}_3$  in order to reveal the spontaneous fission tracks, the sample is totally blackened (Fig. 3B). The acid solution etched all the internal structures and especially the Tomes canals that become visible.

powder. Samples were then irradiated with a neutron flux of  $1.0 \times 10^{16}$  neutrons  $\text{cm}^{-2}$  (ANSTO, Lucas Height, Australia). The micas used as external detector were etched in 40% HF for 40 min at 20 °C in order to reveal the induced fission tracks. To calculate the U concentration from induced fission tracks, CN5 glass was used as dosimeter with a zeta value of  $349 \pm 4.9$  (A–E. Lebatard), obtained on Mont Dromedary apatite standards ( $98.7 \pm 0.6$  Ma) (Hurford and Green, 1983). Fission tracks were counted on the Zeiss Axioplan II microscope, using a magnification of 1250 under dry objectives.

The induced tracks (whose density can be directly related to the U concentration (Fleischer et al., 1965) recorded on the external detector were also used to map the U distribution within the samples (Figs. 5, 6 and 7).

For each data point, induced tracks were counted on a  $100 \times 100 \mu\text{m}$  grid. The error on the calculated U concentration is ca. 10%.

### 3.2. $\alpha$ and $\gamma$ spectrometry

Together with observation of induced fission tracks distribution on the external detectors, U and Th mean concentrations were measured using  $\alpha$  and  $\gamma$  spectrometry. Radiochemistry and  $\alpha$  spectrometry were conducted in the Laboratoire des Sciences du Climat et de l'Environnement (LSCE) in Gif sur Yvette (France) while  $\gamma$  spectrometry were achieved with a high resolution, low background “well-type” Ge detector at the Underground Laboratory in Modane (LSM, Modane, France) (Reyss et al., 1995).

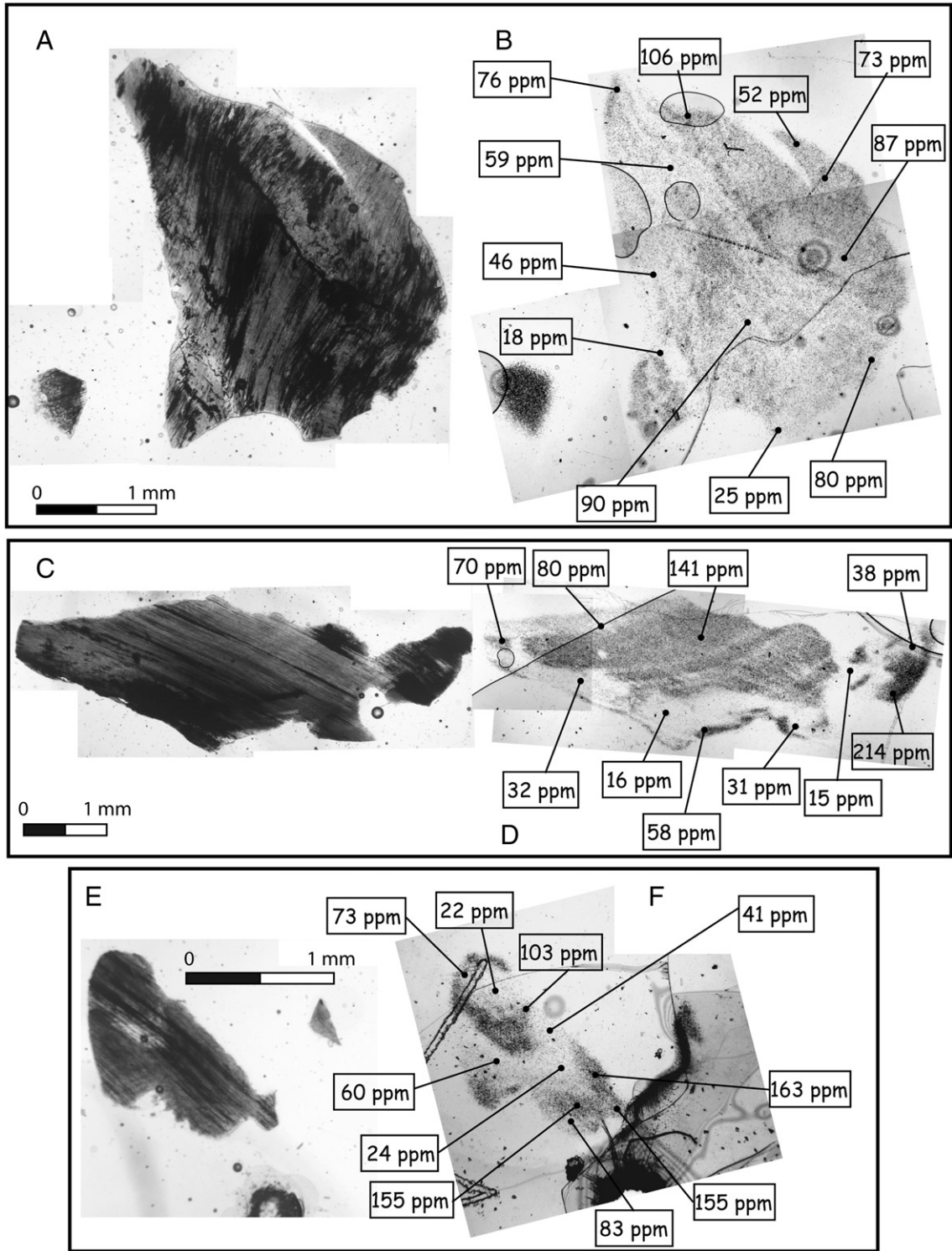


Fig. 5. Determination of the U concentration in Chadian samples using fission tracks. The induced fission tracks on the external detector (right) provide a map of the U content in the sample (left). The induced track density is directly related to the U concentration of the sample. Each U concentration value is given for a  $100\ \mu\text{m} \times 100\ \mu\text{m}$  surface with a maximum uncertainty of 10%. KB3-10, Proboscidian's fossil tooth (KB3, Mio-Pliocene boundary). A, C and E: fragments of the same tooth. B, D and F: induced fission tracks images of these fragments on the external detector after irradiation.

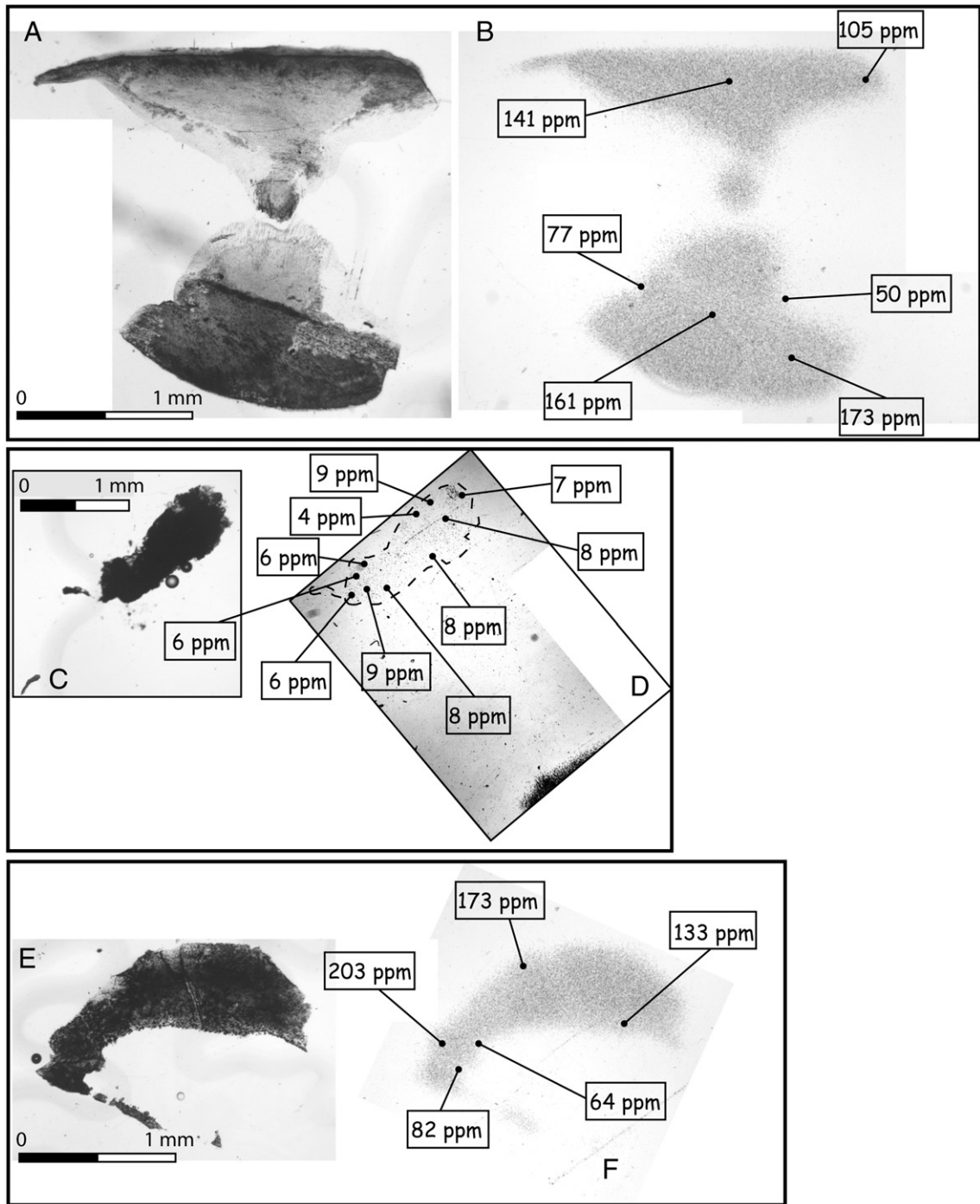


Fig. 6. Same as Fig. 5. TM266 24, Suid fossil tooth (TM266, Late Miocene). A, C, and E: fragments of the same tooth. B, D, and F: induced fission tracks images of these fragments on the external detector after irradiation.

Seven different materials were analysed: enamel, dentine, bone, diagenetic oxides, the sand crust found on some of the Chadian fossils, sand from fossil root tubules from Chad (Toros-Menalla, Fig. 3), and

underground and surface water also from Chad. Enamel was mechanically separated from dentine for samples that presented identified fission tracks (3 from Chad and 1 from France). Teeth and bones surfaces were cleaned

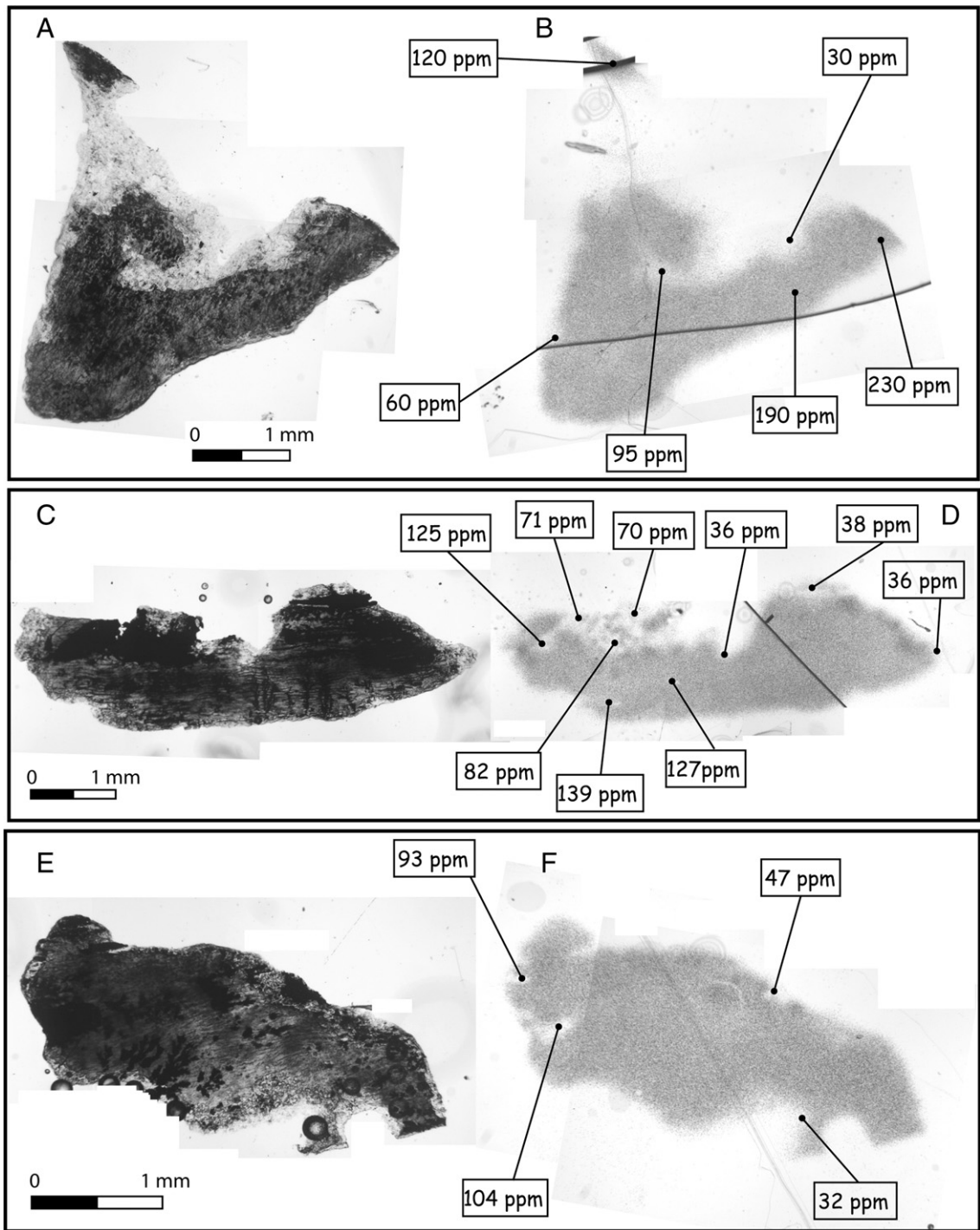


Fig. 7. Same as Figs. 5 and 6. TM90 17, crocodilian fossil osteoderm (TM90, Late Miocene). A, C and E: fragments of the same tooth. B, D and F: induced fission tracks images of these fragments on the external detector after irradiation.

from sand grains by careful scraping of their surface and ultrasonic treatment. The U and Th concentration in groundwater and fossil root tubules was measured to

compare the  $^{234}\text{U}/^{238}\text{U}$  and  $^{230}\text{Th}/^{234}\text{U}$  activity ratios (AR) between the fossils and their surrounding environment. It will provide information on the

diagenetic processes and especially on incorporation of U in the fossils through time. All samples were crushed and weighed. In most cases, the same powder was used for  $\gamma$  and  $\alpha$  spectrometry analysis.

Total  $^{238}\text{U}$  (as  $^{234}\text{Th}$ ) and  $^{226}\text{Ra}$  (as  $^{214}\text{Bi}$  and  $^{214}\text{Pb}$ ) were measured non-destructively on 10–500 mg of dried (at 110 °C) sample material for 1 day using two low-backgrounds, high-efficiency well-type (215 and 430  $\text{cm}^3$ ) Ge  $\gamma$  detectors at the LSM. These detectors are shielded from cosmic radiation by 1700 m of rock and from the radioactivity of the room by 20 cm of old lead.  $^{230}\text{Th}$  was measured at the  $\gamma$  peak energy of 67 keV.  $^{238}\text{U}$  (as  $^{234}\text{Th}$ ) was measured at the  $\gamma$  peak energy of 63.3 keV, and  $^{226}\text{Ra}$  through the short-lived daughters  $^{214}\text{Pb}$  and  $^{214}\text{Bi}$  at 295.2, 352 and 609.3 keV. Measurements were confirmed by summing  $^{238}\text{U}$  (as  $^{234}\text{Th}$  measured at 63.3 keV) and  $^{226}\text{Ra}$  contributions at 185.9 keV. The detectors were calibrated with U and Th NIST standard at 1000 ppm and the standards NIST 4350B, NIST 4353 and IAEA 135 (Turnewitsch et al., 2004).

After the  $\gamma$  analysis, samples were weighted again then ashed at 800 °C for 12 h to remove organic matter. The ashed sample was dissolved in 8 N  $\text{HNO}_3$ , and Al nitrate carrier and  $^{232}\text{U}$  and  $^{228}\text{Th}$  tracer solutions were added. Methods for separation of U and Th, using an ion exchange column, are fully described in Wild and Steffan (1991). Thorium and Uranium were plated on aluminium foil and counted by  $\alpha$ -spectrometry with a grid-chamber. The ages were calculated, when possible, using an iterative computer program (e.g. Ivanovich and Harmon, 1992).

Finally, to separate the diagenetic oxides from enamel and dentine, both materials were weighed independently and leached following the method developed by Sharma and Somayajulu (1979). Leaching with 10% hydroxylamine hydrochloric acid ( $\text{NH}_2\text{-OHHCl}$ ) dissolved the authigenous components of the sample. After 3 successive leachings, the residual solid fraction was washed and dried before  $\gamma$  spectrometry analysis. The leached fraction containing authigenous metals was then prepared for U measurement using the  $\alpha$  spectrometer in LSCE.

### 3.3. Secondary ion mass spectrometry

After fission track analysis, thin sections were polished down to 30  $\mu\text{m}$  to remove the superficial structures revealed by etching. The samples were then coated with carbon and gold. Measurements were done at ISTEEM (Montpellier) on a Cameca IMS4F with an  $\text{O}^-$  extraction flux. The gold and carbon coating was

first eliminated from the analysis area using a 10 nA/15 kV flux during 10 min. As no natural standard samples with known concentrations were available,  $^{30}\text{Si}$  measurements on standard silicate glass SRM610 were used as internal reference. 250 $\times$ 250  $\mu\text{m}$  greyscale images were obtained on key areas determined from FTA. The colour scale of each image is normalized to  $^{30}\text{Si}$ . The maximum relative concentration given for each element in Figs. 8 and 9 corresponds to the brightest point. As absolute concentrations are not calculated, these images can only be used to localize the various elements within the sample and to provide a relative idea of their abundance.

Major elements ( $^{27}\text{Al}$ ,  $^{31}\text{P}$ ,  $^{30}\text{Si}$ ,  $^{40}\text{Ca}$  and  $^{55}\text{Mn}$ ) were measured for 3.5 min and trace elements ( $^{232}\text{U}$  and  $^{238}\text{U}$ ) for 30 min using a 1 nA/15 kV current.

## 4. Results

### 4.1. Fission tracks analysis

Only a small number of the studied samples (all sorts of material considered) showed few recognizable spontaneous fission tracks (a rhinoceros tooth (MH4), a Suidae tooth (TM266-24), a Proboscidian tooth (KB3-10) and a piece of crocodile osteodermis (TM90-17)).

The density of spontaneous fission tracks that should be observed in a sample can be calculated from the age of the sample and the U concentration (see Appendix A for the detailed calculation method). For example, a Chadian fossil from site TM266, with a biostratigraphic age of 7 Ma and a mean U concentration of 100 to 200 ppm should contain between 70 and 130 fission tracks on a 100 $\times$ 100  $\mu\text{m}$  surface.

In mammalian teeth, the internal structures are the first major obstacle for fission track counting (Figs. 2 and 4). Furthermore, in fossils largely affected by diagenesis which contain a high proportion of oxides both within the fossil structure and in late mechanical fractures, diagenetic minerals can also hide the fission tracks (Fig. 1). From optical microscope observation, it appears that aprismatic enamel from reptile teeth is more adequate for fission track observation. This material does not contain visible internal structures and only secondary mechanical cracks occur.

The 4 samples that showed spontaneous fission tracks have been irradiated to estimate their U concentration and distribution.

Figs. 5, 6 and 7 show Chadian teeth fragments and their corresponding images on the external detector. Areas where the fossil sample was very thin due to polishing have been excluded from the following

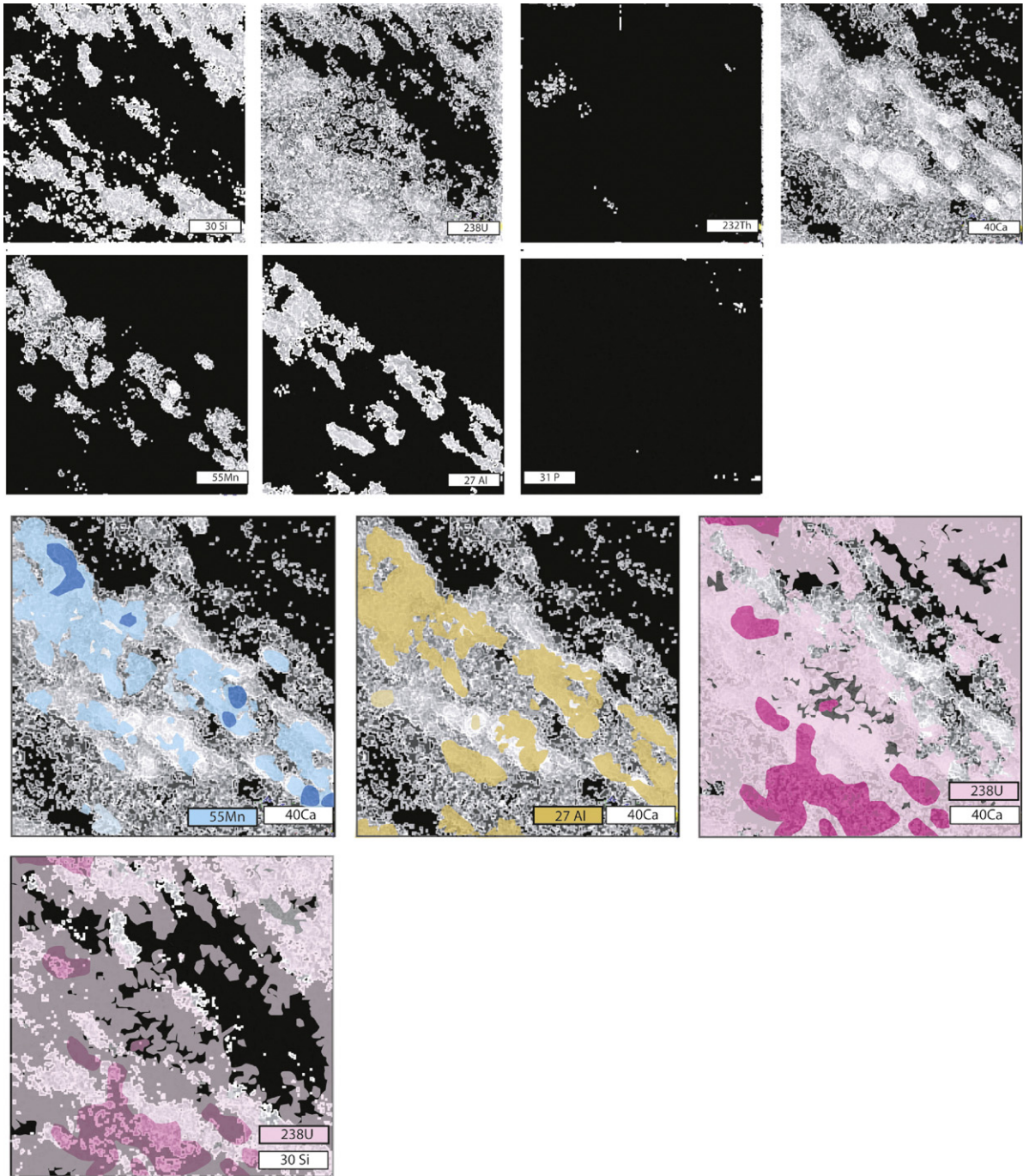
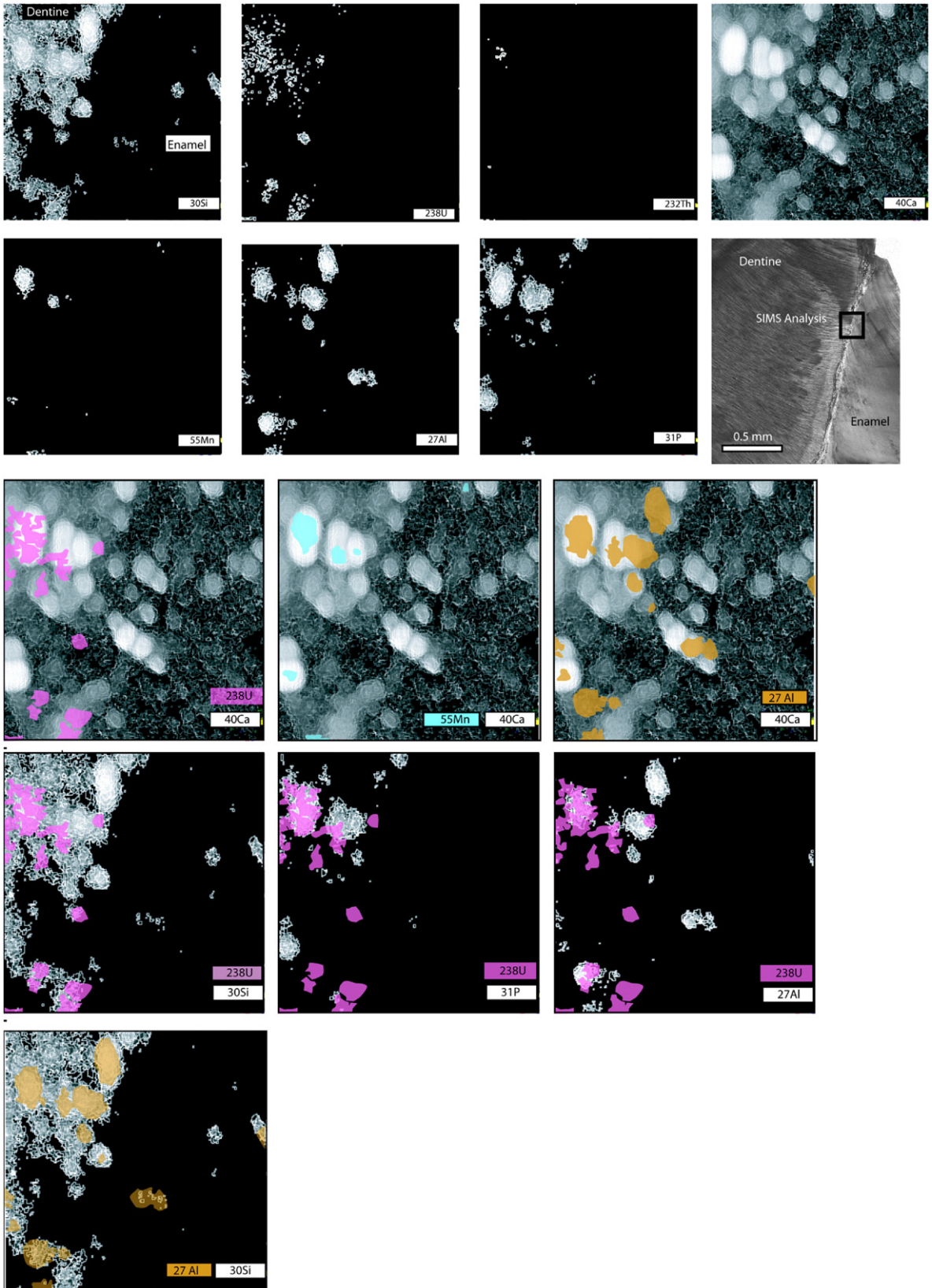


Fig. 8. Top: SIMS raw images of  $^{30}\text{Si}$ ,  $^{238}\text{U}$ ,  $^{232}\text{Th}$ ,  $^{40}\text{Ca}$ ,  $^{55}\text{Mn}$ ,  $^{27}\text{Al}$  and  $^{31}\text{P}$  in a  $250 \times 250 \mu\text{m}$  area of a TM90-17 crocodilian osteoderm. In each individual image brighter colours represent higher relative concentration but the absolute concentration of each element was not calculated. These images can only be used to localize the various elements within the sample. See text for complete discussion. Bottom: correlations between  $^{55}\text{Mn}/^{40}\text{Ca}$ ,  $^{27}\text{Al}/^{40}\text{Ca}$ ,  $^{238}\text{U}/^{40}\text{Ca}$  and  $^{238}\text{U}/^{30}\text{Si}$ .

interpretation because they might not be representative of the samples. Induced fission tracks (and thus U) are observed on the whole surface corresponding to the

fossil but their distribution is not homogeneous. In most images, areas of low induced tracks density correspond to high concentration of oxides within the samples (see



for example on Fig. 6C and D). Calculated U concentrations vary from ca. 10 ppm to ca. 200 ppm with no apparent differences between the species and the localities. Those results are consistent with the mean 100 ppm U concentration obtained from preliminary  $\gamma$  mass spectrometry analysis on some of the Chadian fossils.

Sample MH4 (Burdigalian rhinoceros tooth), which contains a lower amount of oxides compared to the Chadian samples, has a mean U concentration of ca. 60 ppm.

#### 4.2. $\alpha$ and $\gamma$ spectrometry

Results ( $2\sigma$  error) are presented in Table 1. Sample MH4 shows U concentration of ca. 64 ppm in dentine and ca. 36 ppm in enamel. As expected from FTA samples from Chad have higher U concentrations that range from 90 to 280 ppm, the highest values being attained in Kossom Bougoudi (KB3-10) and in one site in Toros-Menalla (TM90-17) (Fig. 3). In all teeth samples (from Chad and from France), the U concentration in dentine is two times higher than in enamel. The  $^{234}\text{U}/^{238}\text{U}$  activity ratio (AR) values in teeth appear constant within a site (see site TM266 in Table 1, and Fig. 10) but slightly higher in the oldest TM266 site than in the KB3-10 site. Furthermore, the  $^{234}\text{U}/^{238}\text{U}$  AR values are similar in dentine and enamel. The  $^{230}\text{Th}/^{234}\text{U}$  values are slightly higher in dentine than in enamel. This also seems to correspond to an increase in  $^{232}\text{Th}$  in dentine (Table 1: samples MH4, BK3-10 and TM266-24). It probably reflects a stronger contamination from diagenetic material in dentine than in enamel.

The diagenetic oxides from the Chadian fossils (separated by leaching following the method of Sharma and Somayajulu (1979)) have very low U concentrations varying from 0.4 to 8.1 ppm (see KB3-10E, KB3-10D, TM266-Os2 and TM266-Os4 in Table 1). The leaching method does not allow discriminating between oxides that were incorporated within the fossil structure and oxides that are deposited inside secondary fracture zones. However, the sandy crust coating the teeth and bones present relatively high U contents. This is especially the case for the oldest site (TM266) which gives U concentration for the sandy crust of 132 ppm, equivalent to the concentration in bones and teeth. A root concretion from site TM254 (equivalent in age to

TM266) formed by a coating of diatomitic material and oxides around the plant roots gives U concentration of 55 ppm. However, this sample contains a smaller proportion of oxides than the sandy crust of TM266.

Finally, U measurements have been made on water from Chad. Groundwater from site TM274 (situated less than 10 km from site TM266, Fig. 2), sampled ca. 50 cm below the surface of the ground gives a U concentration of  $6.5 \pm 0.3$  ppb and a  $^{234}\text{U}/^{238}\text{U}$  AR of  $1.3 \pm 0.11$ . This site is situated within a dry desert area where it seldom rains. Similar values have been obtained in the Eastern Desert of Egypt by Dabous et al. (2002). Water from the Salal well (Fig. 2) (collected at ca. 30 m deep) has a much lower U concentration of  $0.18 \pm 0.02$  ppb but a similar  $^{234}\text{U}/^{238}\text{U}$  AR of  $1.37 \pm 0.17$ . Finally the water from the Cheddra semi-permanent lake (Fig. 2) has an intermediate U concentration of  $1.3 \pm 0.1$  ppb and a slightly lower  $^{234}\text{U}/^{238}\text{U}$  AR of  $1.23 \pm 0.11$ . Those two localities are subjected to periodic rain (the Cheddra area being rainier than Salal which is on the edge of the Djurab Erg desert) that may periodically dilute the underground water.

#### 4.3. Secondary ion mass spectrometry

SIMS analysis was performed to correlate  $^{238}\text{U}$  and  $^{232}\text{Th}$  with other elements and to understand the effects of diagenesis on their distribution. Figs. 8 and 9 present characteristic images obtained on bones or osteoderms (Fig. 8: TM90-17 crocodilian osteoderm) and teeth (Fig. 9: TM266-24 suid tooth). Those images do not provide any quantitative information on the individual concentrations but indicate the location and relative abundance variation of each element (see the “Methodology” section for discussion).

$^{30}\text{Si}$  is present in all fossils but in some samples  $^{31}\text{P}$  and generally  $^{40}\text{Ca}$  are still preserved indicating that diagenesis did not completely erase the initial material.  $^{55}\text{Mn}$  and  $^{27}\text{Al}$  which mostly correspond to the oxides are present in areas with high  $^{40}\text{Ca}$  concentration (see Fig. 8). In TM266-24 tooth (Fig. 9), the  $^{27}\text{Al}$  distribution also matches the  $^{30}\text{Si}$  distribution. On Fig. 8, the  $^{238}\text{U}$  distribution and relative concentration match the  $^{30}\text{Si}$  distribution. This is also probably the case on Fig. 9 but the smaller amount of  $^{238}\text{U}$  does not allow a good interpretation of the image. In this case the  $^{238}\text{U}$  distribution may also correlate with  $^{40}\text{Ca}$ ,  $^{27}\text{Al}$  and  $^{31}\text{P}$ .

Fig. 9. Top: SIMS images of  $^{30}\text{Si}$ ,  $^{238}\text{U}$ ,  $^{232}\text{Th}$ ,  $^{40}\text{Ca}$ ,  $^{55}\text{Mn}$ ,  $^{27}\text{Al}$  and  $^{31}\text{P}$  in a  $250 \times 250 \mu\text{m}$  area of a TM266-24 suid tooth. The probed area was chosen in order to analyse both enamel and dentine at the same time (see location of the analysed zone on microphotograph). See text for complete discussion. Bottom: correlations between  $^{238}\text{U}/^{40}\text{Ca}$ ,  $^{55}\text{Mn}/^{40}\text{Ca}$ ,  $^{27}\text{Al}/^{40}\text{Ca}$ ,  $^{238}\text{U}/^{30}\text{Si}$ ,  $^{238}\text{U}/^{31}\text{P}$ ,  $^{238}\text{U}/^{27}\text{Al}$  and  $^{27}\text{Al}/^{30}\text{Si}$ .

Table 1

Uranium and Thorium nuclide concentrations in fossil, sand, concretion and water measured using  $\alpha$  and  $\gamma$  spectrometry

Lab. no.	Statiagraph. age	Description	$^{232}\text{Th}$ (ppm)	U (ppm)		$^{234}\text{U}/^{238}\text{U}$	$^{230}\text{Th}/^{234}\text{U}$	Corresponding age Th (ka)	+/- (ka)
				$\alpha$	$\gamma$				
MH4 E	Up. Burdigalian	Rhinocerotidae, tooth	–	36.2±0.5	–	2.45±0.03	1.34±0.03	≫ 400	–
MH4 D	Up. Burdigalian	Rhinocerotidae, tooth	–	64.1±3.0	–	2.45±0.09	1.62±0.07	≫ 400	–
KB3-10 E	4.5–5.5 My	Proboscidea, tooth	0.11±0.19	177.9±4.7	155.3±5.7	1.45±0.02	0.91±0.01	205.8	16.6/14.4
KB3-10 E ox l	4.5–5.5 My	Proboscidea, tooth	–	1.04±0.1	–	1.35±0.14	–	–	–
KB3-10 E ox r	4.5–5.5 My	Proboscidea, tooth	–	–	150.9±2.6	–	–	–	–
KB3-10 D	4.5–5.5 My	Proboscidea, tooth	1.35±0.42	283.3±6.0	257.8±10.8	1.42±0.01	1.06±0.01	356.1	43.0/30.7
KB3-10 D ox l	4.5–5.5 My	Proboscidea, tooth	–	8.1±0.2	–	1.35±0.03	–	–	–
KB3-10 D ox r	4.5–5.5 My	Proboscidea, tooth	–	–	201.4±1.5	–	–	–	–
KB3-10 sable		Sandy crust	–	–	33.0±1.8	–	–	–	–
TM266-24 E	ca. 7 My	Suidae, tooth	0.2±0.4	91.1±2.8	–	1.50±0.04	1.1±0.05	>260	–
TM266-24 D	ca. 7 My	Suidae, tooth	1.2±0.8	206.4±5.6	188.1±5.3	1.35±0.03	1.23±0.02	≫ 400	–
TM266-13 t	ca. 7 My	Antracoteriidae, tooth	–	73.2±1.7	–	1.57±0.03	1.14±0.02	≫ 450	–
TM266-Bov E	ca. 7 My	Bovidae, tooth	–	123.9±2.7	–	1.57±0.03	1.18±0.02	≫ 450	–
TM266-Os2	ca. 7 My	Mammalia, bones	–	109.9±5.4	120.3±5.8	–	–	–	–
TM266-Os2 ox l	ca. 7 My	Mammalia, bones	–	1.7±0.1	–	1.26±0.09	–	–	–
TM266-Os2 ox r	ca. 7 My	Mammalia, bones	–	–	126.8±6.8	–	–	–	–
TM266-Os4	ca. 7 My	Mammalia, bones	–	–	158.9±12.4	–	–	–	–
TM266-Os4 ox l	ca. 7 My	Mammalia, bones	–	0.4±0.1	–	1.49±0.40	–	–	–
TM266-Os4 ox r	ca. 7 My	Mammalia, bones	–	–	162.0±7.0	–	–	–	–
TM266-Os4 sand	ca. 7 My	Sandy crust	–	–	131.6±3.0	–	–	–	–
TM90-17	ca. 7 My	Crocodylidae, osteoderms	–	–	265.7±3.8	–	–	–	–
R2 TM254	ca. 7 My	Diatomitic root conduit	–	55.2±0.5	–	1.48±0.01	0.059±0.001	<6.5	0.10/0.10
TM274 Eau	Mio-Pliocene	Groundwater	–	0.0065±0.0003*	–	1.30±0.11	–	–	–
Salal Eau		Groundwater	–	0.00018±0.00002*	–	1.37±0.17	–	–	–
Cheddra N Eau	Actual	Lake water	–	0.0013±0.0001*	–	1.23±0.11	–	–	–

Errors are given at  $2\sigma$ . MH stands for Baigneux in France, KB stands for Kossom Bougoudi (Chad), TM stands for Toros-Menalla (Chad). See Fig. 3 for the localization of Kossom Bougoudi, Toros-Menalla, Salas and Cheddra. E: enamel; D: dentine; t: whole fossil tooth (enamel+dentine+oxides); ox l: leached oxides from sample; ox r: residual material after leaching of the diagenetic oxides; \*: concentration values expressed in  $\mu\text{g/l}$ .

Fig. 9 also shows a strong contrast between the dentine (left) and enamel (right), the concentration of the measured elements being much higher in dentine. The

higher concentration of diagenetic elements such as Si in dentine can be explained by the porous structure of the material that allows fluids to circulate more easily than

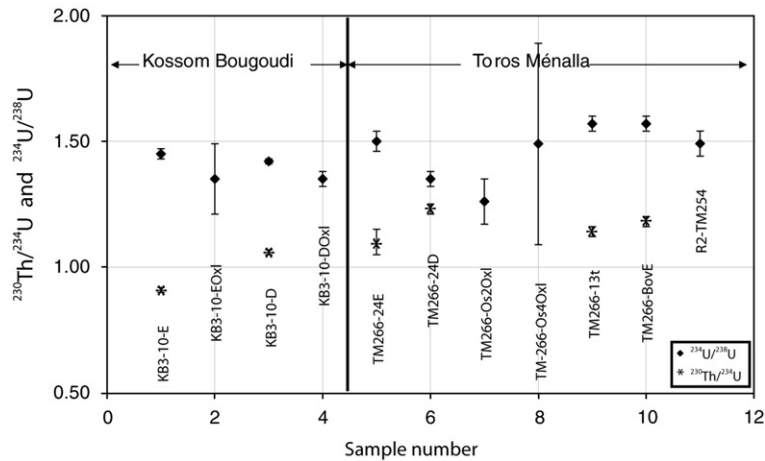


Fig. 10.  $^{234}\text{U}/^{238}\text{U}$  and  $^{230}\text{Th}/^{234}\text{U}$  ratio for the Chadian fossils obtained from  $\alpha$  spectrometry (see text for methodological details). Kossom Bougoudi are samples from site KB3-10 (Mio-Pliocene boundary) and Toros-Menalla from site TM266 (Late Miocene) (Table 1).

in enamel (e.g. Michel et al., 1995; Millard and Hedges, 1996).

## 5. Discussion

Using fission tracks analysis of biogenic apatite as a fossil dating tool appears difficult. Two major difficulties that will be discussed further arise: a) the internal structure of the fossils as well as the very small size of the individual apatite crystallites tend to hide the spontaneous fission tracks; b) biogenic apatite naturally contains small amount of U (in the order of a few ppb) which imply that only fossils of several 100 Ma, old enough to present few spontaneous fission tracks, may be analysed (Sachs et al., 1980). More importantly, diagenetic processes tend to deeply modify the initial material and especially to bring U from the surrounding environment.

### 5.1. Internal structure of the fossils

The difficulty linked to the complexity of teeth and bones internal structures can be partly solved. Teeth with prismatic enamel or thick prismatic enamel will provide surfaces large enough to observe fission tracks. A slight re-polishing (up to a maximum of 1  $\mu\text{m}$ ) of the surface after etching allows to partially erase the “relief” due to etching of both the hydroxyapatite crystallite boundaries and the numerous channels (Tomes canals, Haversian canals, etc). However, such a protocol potentially erases fission tracks that are present only on the surface (either they were horizontal or they penetrated less than 1  $\mu\text{m}$  below the surface from material situated “above” the section). This can slightly

increase the error on the calculated apatite fission track age by underestimating it. Fission tracks analysis in bones is much more difficult than in teeth since internal structures are more developed and larger. Nonetheless thick bones of large animals might provide adequate surfaces.

### 5.2. Redistribution of uranium during diagenesis

Setting aside the observation difficulties, the ability to apply FTA on fossils relies on several parameters: a) some of the initial hydroxyapatite must be preserved during diagenesis; b) the U concentration acquired by the hydroxyapatite during early diagenesis is high enough (several ppm); c) this U must have been incorporated very shortly after deposition of the fossil in the sediment (i.e. in a period of time shorter than the uncertainty on the FTA age); d) no U must be added or subtracted to the fossil after the initial incorporation event. In this paragraph we discuss the potentiality of all those conditions to be fulfilled.

The fact that potential spontaneous fission tracks could be hidden by internal structures in the samples does not alone explain the small number of tracks observed in our samples. Calculations reported in Appendix A show that for the Chadian fossils, the density of spontaneous fission tracks that should be observed is much higher than what is actually seen in the fossils. Fossilization of bones or teeth is a complex process involving decomposition of organic matter (e.g. Hare, 1980; Rae and Ivanovich, 1986; Pfretzschner, 2004), chemical exchanges with the surrounding environment (e.g. Toots and Parker, 1979; Williams and Marlow, 1987; Millard, 1993; Millard and Hedges,

1996; Pike, 2000; Pike et al., 2002; Pfretzschner, 2004) and conversion of biogenic apatite into inorganic apatite minerals (e.g. Bartsiakos and Middleton, 1992). Two hypotheses can then be tested using the Chadian samples: a) the U concentrations measured in the samples result from either a slow, continuous U uptake during diagenesis or a late (compared to the age of the sample), rapid uptake; b) the U is not associated with the hydroxyapatite phase.

### 5.3. Timing of U uptake

Many researchers have documented the strong affinity of mineral apatite for U (e.g. Arey and Seaman, 1999; Jerden and Sinha, 2003; Krestou et al., 2004). Krestou et al. (2004) showed that hydroxyapatite efficiently ( $\approx 95\%$ ) removes U from solutions in the pH range of 3 to 11. The U concentrations measured in the three water samples (Table 1) is low but compatible with values obtained in similar desert environments (e.g. Dabous and Osmond, 2001; Dabous, 2002). The  $^{234}\text{U}/^{238}\text{U}$  AR of the water samples is slightly lower but close to the one observed in the fossil samples (Table 1) indicating that the fossils and the surrounding environment are mostly in equilibrium.

The  $^{230}\text{Th}/^{234}\text{U}$  ratio measured in the fossils varies from 0.91 to 1.23 (Table 1 and Fig. 10). This indicates that either significant  $^{230}\text{Th}$  has been produced within the fossils by  $^{234}\text{U}$  decay or that  $^{234}\text{U}$  has been lost through leaching into the surrounding groundwater. A phase of U uptake followed by a period of loss of some of that U through leaching will leave an excess of the immobile  $^{230}\text{Th}$  daughter product, leading to a  $^{230}\text{Th}/^{234}\text{U}$  ratio greater than the theoretical equilibrium value (e.g. Rae et al., 1989; Pike et al., 2002; Hoffmann and Mangini, 2003).

SIMS images indicate that, when detected,  $^{232}\text{Th}$  is located in discrete areas, generally associated with Mn oxides (Figs. 8 and 9). Williams and Marlow (1987) showed that Th is not incorporated in bones during early diagenesis, and that Th diffusion within fossil bones is very slow. It implies that Th uptake in the samples is a long term process and that  $^{230}\text{Th}$  has most likely been produced in situ, even if a small proportion may have been incorporated during diagenesis. Consequently, U must also have been incorporated (and possibly partially leached) during several episodes corresponding to variations in the redox condition of the surrounding environment (e.g. Millard and Hedges, 1996). All the Chadian fossils are situated inside the lake Mega-Chad basin. Regular flooding of the Chadian desert during formation of mega-lake episode (e.g. Schneider, 1994; Schuster, 2002) followed by evaporation and a return to

dry conditions would be one way to modify the redox conditions of the fossils' environment.

### 5.4. Uranium enrichment in diagenetic oxides

One potential process to artificially increase the U concentration within the fossils is the co-precipitation of U with oxide minerals or other naturally occurring mineral phases such as carbonates and silicates (e.g. Reeder et al., 2000; Duff et al., 2002). U has a high affinity for Fe-oxide minerals. In the geologic environment, U may first sorb to Fe-oxides. Then, as Fe-oxides undergo weathering and microbial interactions, they may dissolve and re-precipitate. During these mineral formation processes, U could be incorporated in the Fe-oxides over long periods of time (e.g. Frederickson et al., 2000; Duff et al., 2002).

The Fe-oxide rich sand crust that covers TM266 fossils has a high U concentration of about 132 ppm (TM266-Os4-sand) whereas the oxide-poor sand that covers KB3 fossils (KB3-10-sand) and the slightly more oxidized root conduit from TM254 (R2 TM254) have a much lower U concentration of about 33 ppm and 55 ppm, respectively (Table 1). Sample KB3-10-sand is younger compared to the other two, which could explain the difference in U concentration. On the contrary, samples R2-TM254 and TM266-Os4-sand have the same stratigraphic age and very different U concentration. The amount of U in the sand immediately surrounding the fossil samples thus appears to be correlated with the oxides concentration and support the hypothesis of co-precipitation of U and Fe-oxides around the fossils.

However, the FTA shows a complete lack of induced fission tracks in oxides-rich zones of the fossils, indicating a very low U concentration (Fig. 6). This is further attested by the very low U concentration obtained by  $\alpha$  spectrometry of the oxide fraction of the samples (Table 1: KB3-10 Eox 1, TM266-Os2-ox 1 and TM266-Os4-ox 1).

It is thus obvious that contrarily to the situation in the surrounding sand crust, diagenetic oxides are not the main U reservoirs in the fossil samples. Precipitation of oxide phases inside the bone structure occurs during the very early diagenetic phase (relatively to the age of the fossil) together with degradation of organic matter, especially collagen (e.g. Newesely, 1989; Pfretzschner, 2004). Like already proposed by Millard and Hedges (1996), our results seem to indicate that this early diagenetic phase has only a negligible effect on the total U uptake of the fossil. At least the oxides precipitated during this phase have no apparent effect on the increase of the U concentration.

### 5.5. Silicification of fossil material and U uptake

Chadian fossils are highly silicified indicating warm and dry, near surface fossilisation conditions (Pfretzschner, 2004). Fig. 9 shows a higher  $^{30}\text{Si}$  concentration within the dentine than in the enamel, correlated with the higher U concentration in dentine (Table 1 and Fig. 9). Silicification of fossil material is a late diagenetic process (Pfretzschner, 2004) and the clear association between  $^{238}\text{U}$  and  $^{30}\text{Si}$  (Figs. 8 and 9) indicates that U uptake certainly continued during the latest fossilisation stages. Access to the internal structure of the tooth is easier in the porous dentine than in the enamel which explains the highest U and Si concentration in the former one (Michel et al., 1997). The distribution of the induced fission tracks on the external detectors (Figs. 5, 6 and 7) indicates that U is not equally distributed in the sample. It appears that longterm diagenesis which leads to mineral substitutions inside the fossils (replacement of hydroxyapatite by calcite and quartz) induces large heterogeneities in the U distribution. This is a major deviation from the Millard and Hedges (1996) DA model that predicts a homogeneous distribution of U in the sample after a period of several 100 kyr.

## 6. Conclusion

Fission tracks analysis of hydroxyapatite fossils is very difficult. As mentioned by Sachs et al. (1980) fossils are made of small apatite micro-crystals whose joints are strongly attacked during the etching phase of the fission track samples preparation, partially or totally blackening the sample. Furthermore, if the internal structure of the conodonts used by Sachs et al. (1980) was relatively simple, bones and teeth from mammals or reptiles contains numerous canals (e.g. Tomes and Haversian canals) which again are strongly attacked during etching. These observation difficulties can be partially solved by using aprismatic enamel or by slightly re-polishing the surface of the samples after etching. However, absolute dating of fossils using the U-series dating is also impeded by the diagenetic processes.

If the early diagenetic stages do not play an important role in the uptake of U, this element seems to be incorporated and/or leached from the fossil over very long periods of time. The “pulses” of U enrichment or leaching probably correspond to changes of redox conditions in the environment. In the example of the Chadian fossil these changes are linked to the numerous fluctuations of the water level within the extensive Lake Chad basin.

Finally the longterm distribution of the U in fossil samples mainly corresponds to diagenetic development of authigenic minerals such as calcite and quartz. In this respect it cannot be described by the DA model of Millard and Hedges (1996). Because uptake and loss of U in fossil bones and teeth is such a very complicated mechanism it appears that FTA dating of Myrs old fossils cannot be reasonably achieved unless fossilization conditions are very stable and known in great detail.

## Acknowledgments

We thank the Chadian Ministère de l'Education Nationale (CNAR and Université de N'Djamena), the French Ministère des Affaires Etrangères (SCAC, N'Djamena and DCSUR, Paris) and Ministère de l'Education Nationale et de la Recherche (Programme Eclipse, CNRS and Université de Poitiers). We are grateful for financial support from the NSF program Revealing Hominid Origins Initiative and to the Mission Paléanthropologique Franco-Tchadienne technical team for its help during field work. We also express our consideration to Ch. Nevado (ISTEEM, Université Montpellier) for the numerous thin sections and to S. Sen (Muséum National d'Histoire Naturelle, Paris) for providing a large collection of samples. Finally we want to acknowledge the help of two anonymous reviewers as well as Pr. C. Göpel and Pr. B. Bourdon for their constructive review of the manuscript.

## Appendix A. Calculation of the expected number of fission tracks in a sample

The density of fission tracks that can be expected in a sample of known age and U concentration can be calculated using:

$$P_{\text{FT}} = \frac{\lambda_{\text{F}}}{\lambda_{\text{T}}} {}^{238}\text{U} (e^{\lambda_{\text{T}}t} - 1) \quad (1)$$

where  $\lambda_{\text{F}}$  is the  $^{238}\text{U}$  decay constant ( $8.46 \times 10^{-17}$ ),  $\lambda_{\text{T}} = \lambda_{\text{F}} + \lambda = 8.46 \times 10^{-17} + 1.55125 \times 10^{-10}$  with  $\lambda$  the alpha decay constant. As  $\lambda_{\text{F}} \ll \lambda$  it is generally considered that  $\lambda_{\text{T}} \approx \lambda$ .  $t$  is the age of the sample and  $^{238}\text{U}$  is the number of  $^{238}\text{U}$  atoms per  $\text{cm}^3$  calculated from

$${}^{238}\text{U} = \frac{U_{(\text{ppm})} \times I \times A \times \rho}{10^6 \times 238} \quad (2)$$

where  $U_{(\text{ppm})}$  is the measured U concentration in the sample,  $A$  is the Avogadro constant,  $\rho$  is the apatite density and  $I = \frac{137.88}{138.88}$ .

The maximum number of fission tracks ( $N_{FT}$ ) to be expected on a definite observation surface can then be calculated using:

$$N_{FT} = P_{FT} \times a \times L \quad (3)$$

where  $a$  is the observation area and  $L$  is the maximum length of the fission track.

As an example, samples from Toros-Menalla have an estimated age of 7 Ma and a U concentration of 100 to 200 ppm (Table 1). Using an apatite density of 3.2,  $^{238}\text{U}$  will then vary between  $8.0392 \times 10^{17}$  and  $1.6078 \times 10^{18}$  atoms per  $\text{cm}^3$ . The corresponding  $P_{FT}$  will vary from  $476.34 \times 10^6$  to  $952.68 \times 10^6$  atoms for  $1 \text{ cm}^3$ .

The number of fission tracks ( $N_{FT}$ ) to be expected on a typical counting surface of  $100 \mu\text{m} \times 100 \mu\text{m}$  and using a maximum track length of  $14 \mu\text{m}$  will then vary between 68 and 133 tracks.

## References

- Arey, J.S., Seaman, J.C., 1999. Immobilization of uranium in contaminated sediments by hydroxyapatite addition. *Environmental Science and Technology* 33, 337–342.
- Barbarand, J., Carter, A., Wood, I., Hurford, T., 2003. Compositional and structural control of fission-track annealing in apatite. *Chemical Geology* 198, 107–137.
- Bartsiokas, A., Middleton, A.P., 1992. Characterization and dating of recent and fossil bone by X-ray diffraction. *Journal of Archaeological Science* 19 (1), 63–72.
- Brunet, M., Guy, F., Pilbeam, D., Lieberman, D.E., Likius, A., Mackaye, H.T., Ponce De Leon, M., Zollikofer, C., Vignaud, P., 2005. New material of earliest hominid from the Upper Miocene of Chad. *Nature* 434, 752–755.
- Coyle, D.A., Wagner, G.A., 1998. Positioning the Titanite fission track partial annealing zone. *Chemical Geology* 149, 117–125.
- Dabous, A.A., 2002. Uranium isotopic evidence for the origin of the Bahariya iron deposits, Egypt. *Ore Geology Reviews* 19, 165–186.
- Dabous, A.A., Osmond, J.K., 2001. Uranium isotopic study of artesian and pluvial contributions to the Nubian aquifer, western desert, Egypt. *Journal of Hydrology* 243, 242–253.
- Dabous, A.A., Osmond, J.K., Dawood, Y.H., 2002. Uranium/Thorium isotope evidence for ground-water history in the Eastern Desert of Egypt. *Journal of Arid Environments* 50, 343–357.
- Dahl, S.D., 1997. A crystal-chemical basis for Pb retention and fission track annealing systematics in U-bearing minerals, with application for geochronology. *Earth and Planetary Science Letters* 150, 277–290.
- Duff, M.C., Urbanik Coughlin, J., Hunter, D.B., 2002. Uranium coprecipitation with iron oxide minerals. *Geochimica Cosmochimica Acta* 66 (20), 3533–3547.
- Eggs, S., Grün, R., Pike, A.W.G., Shelley, M., Taylor, L., 2003.  $^{238}\text{U}$ ,  $^{232}\text{Th}$  profiling and U-series isotope analysis of fossil teeth by laser ablation-ICPMS. *Quaternary Science Reviews* 22, 1373–1382.
- Fleischer, R.L., Price, P.B., Walker, R.M., 1965. Tracks of charged particles in solid. *Science* 149, 363–393.
- Frederickson, J.K., Zachara, J.M., Kennedy, D.W., Duff, M.C., Gorby, Y.A., Li, S.W., Krupka, K.M., 2000. Reduction of U(VI) in goethite ( $\alpha\text{-FeOOH}$ ) suspensions by a dissimilatory metal-reducing bacterium. *Geochimica et Cosmochimica Acta* 64, 3085–3098.
- Gleadow, A.J.W., Brown, W., 2000. Fission-track thermochronology and the long-term denudational response to tectonics. In: Summerfield, M.A. (Ed.), *Geomorphology and Global Tectonics*. Wiley & Sons, Chichester, England.
- Green, P.F., Duddy, I.R., Gleadow, A.J.W., Laslett, G.M., Tingate, P.R., 1986. Thermal annealing of fission tracks in apatite, 1-A qualitative description. *Chemical Geology* 59, 234–253.
- Hare, P.E., 1980. Organic geochemistry of bone and its relation to survival of bone in the natural environment. In: Behrensmeyer, A.K., Hill, A.P. (Eds.), *Fossils in the Making*. University of Chicago Press, Chicago, pp. 208–219.
- Hoffmann, D., Mangini, A., 2003. A method for coupled ESR/U-series dating of teeth showing post-depositional U-loss. *Quaternary Science Reviews* 22, 1367–1372.
- Hurford, A.J., 1990. Standardization of fission track dating calibration: Recommendation by the Fission track Working Group of the I.U.G.S. Subcommittee on Geochronology. *Chemical Geology* 80, 171–178.
- Hurford, A.J., Green, P.F., 1983. The zeta age calibration of fission-track dating. *Chemical Geology. Isotope Geoscience Section* 1, 285–317.
- Ivanovich, M., Harmon, R.S., 1992. Appendix A. Derivation of the expressions for the  $^{234}\text{U}/^{238}\text{U}$  and  $^{230}\text{Th}/^{234}\text{U}$  activity-ratio age equations. Uranium-Series disequilibrium: applications to Earth, Marine, and Environmental sciences. Clarendon Press, Oxford, pp. 779–781.
- Iyengar, G.V., Kollmer, W.E., Bowen, H.J.M., 1978. *The Elemental Composition of Human Tissue and Body Fluids*. Springer-Verlag, New York.
- Jerden, J.L., Sinha, A.K., 2003. Phosphate based immobilization of uranium in an oxidizing bedrock aquifer. *Applied Geochemistry* 18, 823–843.
- Jolivet, M., Brunel, M., Seward, D., Xu, Z.h., Yang, J., Roger, F., Tapponnier, P., Malavieille, J., Arnaud, N., Wu, C., 2001. Mesozoic and Cenozoic tectonics of the northern edge of the Tibetan plateau: fission-track constraints. *Tectonophysics* 343 (1–2), 111–134.
- Jolivet, M., Ritz, J.-F., Vassallo, R., Larroque, C., Braucher, R., Todbileg, M., Chauvet, A., Sue, C., Arnaud, N., De Vicente, R., Arzhanikova, A., Arzhanikov, S., 2007. The Mongolian summits: An uplifted, flat, old but still preserved erosion surface. *Geology* 35 (10), 871–874.
- Krestou, A., Xenidis, A., Panias, D., 2004. Mechanism of aqueous uranium(VI) uptake by hydroxyapatite. *Minerals Engineering* 17, 373–381.
- Kusnir, I., Moutaye, H.A., 1997. Ressources minérales du Tchad: une revue. *Journal of African Earth Sciences* 24 (4), 549–562.
- Michel, V., Ildefonse, P., Morin, G., 1995. Chemical and structural changes in *Cervus elaphus* tooth enamels during fossilization (Lazaret cave): a combined IR and XRD Rietveld analysis. *Applied Geochemistry* 10, 145–159.
- Michel, V., Falguères, C., Yokoyama, Y., 1997. Teneur en uranium et datation U–Th des tissus osseux et dentaires fossiles de la grotte de Lazaret. *Comptes Rendus Académie Sciences Paris (II)* 325, 381–387.
- Michel, V., Locht, J.-L., Antoine, P., Masaoudi, H., Falguères, C., Yokoyama, Y., 1999. Datation ESR/U–Th combinée des restes fauniques du site moustérien de plein air de Beauvais. *Comptes Rendus Académie Sciences Paris (II)* 329, 369–375.
- Millard, A.R., 1993. Diagenesis of archeological bone: the case of uranium uptake. D. Phil. thesis, University of Oxford. England.

- Millard, A.R., Hedges, R.E.M., 1996. A diffusion-absorption model of uranium uptake by archaeological bone. *Geochimica et Cosmochimica Acta* 60 (12), 2139–2152.
- Newesely, H., 1989. Fossil bone apatite. *Applied Geochemistry* 4, 233–245.
- O’Sullivan, P.B., Parrish, R.R., 1995. The importance of apatite composition and single-grain ages when interpreting fission track data from plutonic rocks: a case study from the Coast Ranges, British Columbia. *Earth and Planetary Science Letters* 132, 213–224.
- Pfretzschner, H.-U., 2004. Fossilization of Haversian bone in aquatic environments. *Comptes Rendus Palevol* 3, 605–616.
- Pike, A.W.G., 2000. U-series dating of archaeological bone using TIMS. D. Phil. thesis, University of Oxford, U.K.
- Pike, A.W.G., Hedges, R.E.M., 2001. Sample geometry and U uptake in archaeological teeth: implications for U-series and ESR dating. *Quaternary Science Reviews* 20, 1021–1025.
- Pike, A.W.G., Hedges, R.E.M., Van Calsteren, P., 2002. U-series dating of bone using the diffusion-adsorption model. *Geochimica et Cosmochimica Acta* 66 (24), 4273–4286.
- Rae, A.M., Ivanovich, M., 1986. Successful application of uranium series dating of fossil bone. *Applied Geochemistry* 1, 419–426.
- Rae, A., Hedges, R.E.M., Ivanovich, M., 1989. Further studies for uranium-series dating of fossil bones. *Applied Geochemistry* 4, 331–337.
- Reeder, R.J., Nugent, M., Lamble, G.M., Tait, C.D., Morris, D.E., 2000. Uranyl incorporation into calcite and aragonite: XAFS and luminescence studies. *Environmental Science and Technology* 34, 638–644.
- Reyss, J.L., Schmidt, S., Legeleux, F., Boute, P., 1995. Large, low background well-type detectors for measurements of environmental radioactivity. *Nuclear Instruments and Methods in Physical Research A* 357, 391–397.
- Sachs, H.M., Denking, M., Bennett, C.L., Harris, A.G., 1980. Radiometric dating of sediments using fission tracks in conodonts. *Nature* 288, 359–361.
- Schneider, J.-L., 1994. *Le Tchad depuis 25 000 ans, Géologie, Archéologie, Hydrologie*. Collection Préhistoire, Masson Ed.
- Schuster, M., 2002. *Sédimentologie et paléocéologie des séries à vertébrés du paléolac Tchad depuis le Miocène supérieur*. PhD Thesis unpublished, University Louis Pasteur, Strasbourg, France, 152 pp.
- Sharma, P., Somayajulu, B.L.K., 1979. Growth rates and composition of two ferromanganese nodules from the central north Pacific. *Coll. Int. du C.N.R.S., La genèse des nodules de Manganèse*, ed. du C.N.R.S, Paris, No. 289, 281–289.
- Sharma, K.K., Choubey, V.M., Sharma, O.P., Nagpaul, K.K., 1981. Uranium distribution in siwalik vertebrates using fission track technique. *Journal of the Geological Society of India* 22, 92–97.
- Sobel, E.R., Oskin, M., Burbank, D., Mikolaichuk, A., 2006. Exhumation of basement-cored uplifts: example of the Kyrgyz Range quantified with apatite fission track thermochronology. *Tectonics* 25. doi:10.1029/2005TC001809.
- Tagami, T., Shimada, C., 1996. Natural long-term annealing of the zircon fission track system around a granitic pluton. *Journal of Geophysical Research* 101 (B4), 8245–8255.
- Tagami, T., Carter, A., Hurford, A.J., 1996. Natural long-term annealing of the zircon fission-track system in Vienna Basin deep borehole samples: constraints upon the partial annealing zone and closure temperature. *Chemical Geology* 130, 147–157.
- Toots, H., Parker, R.B., 1979. Factors affecting fluorine content of fossil bones and teeth. *Contribution to Geology at the University of Wyoming* 18, 69–70.
- Turnewitsch, R., Reyss, J.-L., Chapman, D.C., Thomson, J., Lampitt, R.S., 2004. Evidence for a sedimentary fingerprint of an asymmetric flow field surrounding a short seamont. *Earth and Planetary Science Letters* 222 (3–4), 1023–1036.
- Van Calsteren, P., Thomas, L., 2006. Uranium-series dating applications in natural environmental science. *Earth-Science Reviews* 75, 155–175.
- Wild, E., Steffan, I., 1991. Isolation of Uranium and Thorium for age determination of fossil bones by Uranium series method. *Radiochimica Acta* 54, 85–89.
- Williams, C.T., Marlow, C.A., 1987. Uranium and Thorium distribution in fossil bones from Olduvai gorge, Tanzania and Knam, Kenya. *Journal of Archaeological Science* 14, 297–309.